JGR Solid Earth

RESEARCH ARTICLE
10.1029/2022JB024920

Thermally Induced Microcracks in Granite and Their Effect on the Macroscale Mechanical Behavior

J. J. Xu[1], Y. H. Zhang[1], J. Rutqvist[2], M. S. Hu[2], Z. Z. Wang[1], and X. H. Tang[1,3]

[1]School of Civil Engineering, Wuhan University, Wuhan, China, [2]Lawrence Berkeley National Laboratory, Berkeley, CA, USA, [3]Wuhan University Shenzhen Research Institute, Shenzhen, China

Key Points:

- The initiation, propagation, and coalesce of thermally induced microcracks in granites were first observed experimentally in real time
- The coalesce of microcracks between 400 and 600°C mainly induces the sharply decrease of the macroscale strength of granites
- The evolution of microcracks and macroscale strength were reproduced by accurate grain-based modeling with precise microscale parameters

Correspondence to:
X. H. Tang,
xuhaitang@whu.edu.cn

Citation:
Xu, J. J., Zhang, Y. H., Rutqvist, J., Hu, M. S., Wang, Z. Z., & Tang, X. H. (2023). Thermally induced microcracks in granite and their effect on the macroscale mechanical behavior. *Journal of Geophysical Research: Solid Earth*, *128*, e2022JB024920. https://doi.org/10.1029/2022JB024920

Received 7 JUN 2022
Accepted 25 DEC 2022

Author Contributions:
Conceptualization: J. J. Xu, X. H. Tang
Data curation: J. J. Xu, Y. H. Zhang, Z. Z. Wang
Funding acquisition: X. H. Tang
Investigation: J. J. Xu, Y. H. Zhang
Methodology: J. J. Xu, Z. Z. Wang, X. H. Tang
Project Administration: X. H. Tang
Software: J. J. Xu
Supervision: J. Rutqvist, M. S. Hu, Z. Z. Wang, X. H. Tang
Validation: J. J. Xu
Visualization: J. J. Xu
Writing – original draft: J. J. Xu
Writing – review & editing: J. Rutqvist, M. S. Hu, X. H. Tang

© 2023. The Authors.
This is an open access article under the terms of the Creative Commons Attribution License, which permits use, distribution and reproduction in any medium, provided the original work is properly cited.

Abstract Understanding the thermal effects on rock is critical for the exploration of geothermal resources and the temperature-driven evolution of Earth. The macroscale mechanical behavior of granite under thermal loading can be complicated due to microcracking and the heterogeneity of minerals. In this study, the thermally induced microcrack propagation of granite was first observed in real time by an ultrahigh-temperature instrument on an optical microscope. The previous investigation believed that the α–β quartz transition at approximately 573°C leads to a sharp decrease in macroscale mechanical behavior. However, the present experimental results revealed that microcracks initiate at 300°C and coalesce between 400 and 600°C, which is the main reason for the sharp decrease in macroscale mechanical properties of granite. Additionally, an accurate grain-based model based on the mineralogical morphology of granite samples adopted mechanical parameters of minerals obtained from microscale rock mechanical techniques. It is able to well reproduce the process of microcracking and the strength evolution of granite during heating. The numerical results show that the heterogeneity of thermal expansion and mechanical properties of minerals produce local thermal stress concentrations in granite. The uneven tensile-compressive stress between feldspar and quartz and the shear stress around biotite result in the initiation and propagation of microcracks. The present work is potentially useful for understanding and predicting the mechanical behavior of granites under thermal loading with different mineral compositions and microstructures.

Plain Language Summary Investigating the thermal effects on rock is critical for controlling the state of reservoirs during geothermal resource exploitation and understanding the temperature-driven evolution of Earth. It is known that the macroscale mechanical behavior of granite under thermal loading changes due to microcracking and the heterogeneity of minerals. This work developed an experimental system and accurate grain-based modeling method to investigate the microcracking and mechanical behavior of minerals under realistic high-temperature environmental conditions. An ultrahigh-temperature instrument was used for the first real-time observation of thermal-induced cracks in the granite. The accurate grain-based models combined the real mineral composition of granite and the precise mechanical properties of minerals were built to duplicate the microcrack characteristic. It provides a solution to the lack of accuracy and physical meaning in determining parameters for properties at grain scale. The comparison with experiments in respect to microcracking patterns shows a remarkable agreement. Results of experimental observation analysis and numerical simulation revealed that the microcracks initiate at 300°C, then coalesce between 400 and 600°C. The damage accumulation of rock under thermal loading can significantly reduce the physical mechanical properties of the granites.

1. Introduction

Owing to changes in temperature with time in active tectonic setting, for example, melt migration and magma-chamber formation, vast volumes of crustal rock will develop extensive microcracks in response to thermal loading (Johnson et al., 2021), which has a significant influence on their physical and mechanical properties. The damage horizon might occur at depths of 5 km geothermal fields or at greater depths where thermal gradients can reach >120°C/km (Marini & Manzella, 2005). Since granites are considered the target formation for deep geothermal energy, understanding and controlling the mechanical behavior of granites under thermal loading are critical for geothermal exploration from hot dry rock (Aghahosseini & Breyer, 2020; Salimzadeh et al., 2018). Thermally induced cracking has been identified as the cause of the reduced strength and enhanced permeability of rock at high temperatures (Nasseri et al., 2009). Furthermore, the reduction of friction coefficient (Du et al., 2022) at elevated temperatures and pore fluid pressures may potentially promote fault destabilization

or failure under conditions typifying a geothermal reservoir (An et al., 2021, 2022). Therefore, an in-depth understanding of the strength evolution of granite is important for the safe and economical design of deep underground engineering (Wong et al., 2020).

Extensive macroscale laboratory testing has been undertaken to investigate the mechanical behavior and thermally induced failure pattern of granite at high temperatures. The variation in the compressive strength and elastic modulus of granite with temperature has been studied by uniaxial compressive testing (Sha et al., 2020). A series of high-pressure and high-temperature triaxial experiments were carried out to investigate the stress–strain behavior under in situ stress and temperature conditions (Kumari, Ranjith, Perera, Shao, et al., 2017). Fan et al. (2017) conducted an experimental investigation of thermal effects on the dynamic behavior of granite. The relationship between the fracture toughness of granite and temperature was determined using cracked chevron notched Brazilian disk specimens (Nasseri et al., 2009; Z. L. Shao et al., 2021). The effects of thermal loading on the Brazilian tensile strength were studied by Z. H. Li et al. (2017). The macroscale rock mechanics experiments confirmed that thermal-stress-induced cracking contributes to the decrease in rock strength.

A wide variety of experimental techniques have been applied to observe the microcracking of granite under thermal loading. Without applying thermal loading in real time, the number, length, and orientation of microcracks can be directly observed and quantified (Z. H. Li et al., 2020) by scanning electron microscopy (SEM; Nasseri et al., 2009; S. S. Shao et al., 2015; Ündül, 2016) and thin-section optical microscopy (Griffiths et al., 2017; Z. H. Li et al., 2020). However, direct observation techniques have difficulty distinguishing whether microcracks are thermally induced or preexisting due to the inability to observe in situ and in real time (F. Wang & Konietzky, 2022). By applying thermal loading in real time, indirect observation techniques, including monitoring of acoustic emission signals (Griffiths et al., 2018; Nicco et al., 2018; Z. L. Shao et al., 2020; Yang et al., 2020), ultrasound velocity propagation (D. B. Wang et al., 2021), mercury intrusion porosimetry (F. B. Wu et al., 2021), and X-ray computed tomography (CT; Fan et al., 2018; Guo et al., 2017), have been used to describe macroscopic thermal damage, but the derivation of microcracks cannot be directly observed to reveal the underlying mechanisms of the temperature influence on the rock strength.

Because it is difficult to observe microcracks directly in laboratory tests, numerical methods have been developed and applied to visualize the thermal failure process. Jiao et al. (2015) built a 2D discontinuous model for simulating the thermal cracking of brittle rocks based on the discontinuous deformation analysis method. A finite element model was applied to verify the thermal stress in different microstructures with various fabric parameters (Vázquez et al., 2015) and simulate the compression tests carried out on granite at elevated temperatures (S. S. Shao et al., 2015; F. Wang & Konietzky, 2019). Z. H. Zhao (2016) elucidated that the strength reduction of granite mainly results from the increasing thermal stresses and the generation of tensile microcracks by particle-based approach simulation. T. Xu et al. (2017) proposed a thermomechanical numerical model that describes the brittle creep of granite under different temperatures and confining pressures. In these models, the rock microstructures are virtually generated by assuming either a statistical or random distribution of the physical properties of the elements. These assumptions make it difficult to specify the statistical distribution parameters to consider the actual microstructures in rock and may misinterpret the influence of critical local-scale heterogeneities on rock thermal cracking (Zhu et al., 2006). The thermal damage of granite is dependent on the mineralogy, thermal expansion, and elastic properties of the grains. Accurately understanding the physical and mechanical properties of rock-forming minerals is critical for the analysis of microcracks in granites subjected to thermal loading. Although existing digital models can accurately reproduce rock microstructures (F. Wang & Konietzky, 2022; Yu et al., 2015), they still cannot overcome the difficulty of determining microscopic parameters. Therefore, it is difficult to make a meaningful comparison of simulation modeling and experimental results because of the limitations of the in situ observation of microcracks and existing numerical simulations. The relationship between the microscopic damage caused by thermal loading and the changes in the macroscale mechanical properties of rocks remains poorly understood.

In this work, novel experimental and numerical methods were developed in Section 2 to investigate thermally induced microcracking in granite. The accurate grain-based model (AGBM) was generated based on the mineralogical morphology and mechanical parameters obtained from microscale rock mechanics experiments (micro-RME). In Section 3, the initiation and propagation of microcracks in granite subjected to high temperature were observed in real time with microscopic observations. Then, the AGBM was used to simulate the stress state of granites under the temperature between 25°C and 900°C. By comparing with the experimental results,

the validity of the model was confirmed, and the thermal cracking mechanisms were revealed. In Section 4, the proposed model was used to discuss the influence of temperature on the uniaxial compressive strength (UCS) and Young's modulus of granite. Finally, a comprehensive data compilation was presented to analyze the temperature-dependent characteristic of granite properties. This research is beneficial for the optimization of thermal rock fragmentation processes in geothermal engineering.

2. Properties of Minerals and AGBMs

2.1. Nanoindentation

Nanoindentation was applied to measure the mechanical properties of minerals, including elastoplastic and failure properties (Y. C. Li et al., 2021; S. Y. Liu et al., 2022; Y. W. Liu et al., 2022; Luo et al., 2020), to investigate the heterogeneity of granite and provide precise microscale parameters for numerical modeling.

2.1.1. The Principle of Measuring the Elastic Modulus of Minerals

In the nanoindentation test, the elastic modulus E and hardness H of a sample can be derived from the generated load–depth curves. The contact stiffness S can be achieved by the elastic solution relating to the applied loading force P and indentation depth h: $S = \frac{dP}{dh}|h = h_{\max}$, where $h_{\max}$ is the maximum indentation depth. The reduced modulus E_r is calculated as (Sneddon. 1965)

$$E_r = \frac{\sqrt{\pi}}{2\beta\sqrt{A_c}}S \tag{1}$$

where β is a dimensionless correction factor associated with the indenter tip shape ($\beta = 1.05$ is commonly used for Berkovich indenter). A_c is the projected contact area of the indenter on the sample surfaces, which is typically determined by a function of the maximum contact depth h_c: $A_c = f(h_c)$. The contact depth h_c is calculated as $h_c = h_{\max} - \varepsilon\frac{P}{S}$ (ε is a constant that depends on the indenter tip).

The elastic modulus of the samples is calculated by the following equation:

$$E = \left(1 - v^2\right)\left[\frac{1}{E_r} - \frac{1 - v_i^2}{E_i}\right]^{-1} \tag{2}$$

where v and v_i are the Poisson's ratios of the sample and indenter, respectively. E_i is the Young's modulus of the indenter, which is 1,140 GPa.

2.1.2. The Principle of Measuring the Cohesion and Friction Angle of Minerals

The Mohr-Coulomb constitutive model ($\tau = \sigma_n \tan\varphi + c$) is one of the most commonly used criteria for shear strength in rock engineering. Ganneau et al. (2006) proposed a dual indentation technique to assess the cohesion c and friction angle φ of the Mohr-Coulomb model to investigate the failure strength of cohesive-frictional material. Palkovic et al. (2018) applied this scaling relation to study the cohesive-frictional properties of cement paste with different components by nanoindentation experiments. J. J. Xu et al. (2020) employed this method to investigate the influence of water softening on the failure properties of shale.

The hardness is calculated by dividing the applied load P by the area of the contact surface projected on the initial sample surface A_c:

$$H = \frac{P}{A_c} \tag{3}$$

The hardness is primarily a function of the friction angle φ and cohesion c of the material and apex angle θ of the indenter. Therefore, the hardness-to-cohesion ratio depends on only two parameters, the friction angle φ and the tip apex angle θ, is shown in formula given in Equation 4. By studying the property of these dimensionless relations, it is shown that the ratio of two hardness measurements obtained from indentation tests with different apex angles allows one to determine the friction angle φ of the material (Equation 5; Ganneau et al., 2006).

$$\frac{H}{c} = \frac{\delta'(\varphi,\theta)}{\tan\varphi} = \frac{1}{\tan\varphi}\sum_{k=1}^{k=N}(a_k\tan\varphi)^k \tag{4}$$

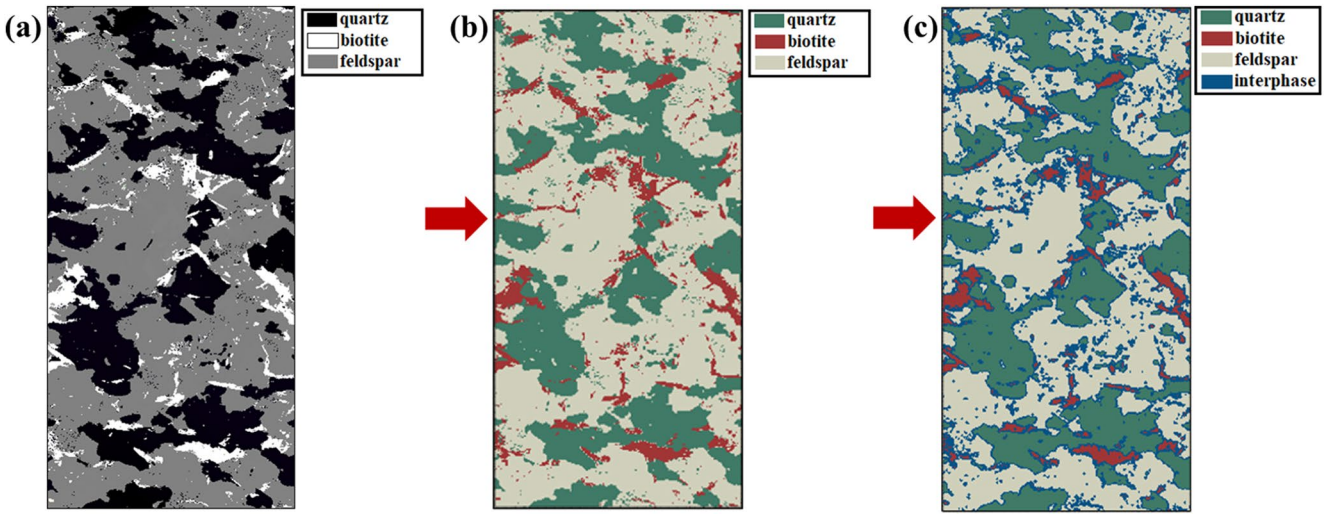


Figure 1. Generation of the micro-RME-based model: (a) TIMA images, (b) mineral mechanical properties are set according to mineral types, and (c) the interphase-element is inserted between different minerals.

$$\frac{H_{\mathrm{B}}}{H_{\mathrm{CC}}} = \frac{\delta'(\varphi, \theta_{\mathrm{B}})}{\delta'(\varphi, \theta_{\mathrm{CC}})} \tag{5}$$

In this work, a Berkovich indenter and cube-corner indenter were applied in combination with the yield design theorems, where a_k are fitting coefficients that depend on the geometry of the indenters. An $N = 6$ power expression (i.e., fifth-order in tan φ) fits the function of H/c relations perfectly. The values of fitting coefficients for the Berkovich indenter $a_k(\theta_{\mathrm{B}})$ and cube-corner indenter $a_k(\theta_{\mathrm{CC}})$ are given in the literature (Ganneau et al., 2006). Equation 5 provides a means of assessing φ from the difference in hardness between a Berkovich indentation test (H_{B}) and a cube-corner indentation test (H_{CC}), which confirmed that there is a unique relation between the hardness ratio ($H_{\mathrm{B}}/H_{\mathrm{CC}}$) and the friction angle φ. Once the friction angle is determined, it is possible to determine the cohesion from the H_{B}/c curves displayed in Ganneau et al. (2006).

2.2. Accurate Grain-Based Models

The AGBM combined real mineral composition of granite and precise mechanical properties of minerals were built to duplicate the microcrack characteristic. It provides a solution to the lack of accuracy and physical meaning in determining parameters for properties at grain size scale. The mechanical properties of rock-forming minerals and interphase were measured and calibrated in Sections 2.3 and 2.4, respectively.

An accurate grain-based numerical model (see Figure 1) with a height of 20 mm and a width of 10 mm was applied to simulate uniaxial compression of granite (Tang et al., 2022). This model was then used for calibrating microparameters of interphase that could not be directly measured by tests, as well as for investigating the evolution of macroscale mechanical properties of granite. The microstructure of granite was obtained by a TESCAN Integrated Mineral Analyzer (TIMA), which can quantitatively analyze rock composition based on SEM in backscattered electron (BSE) imaging mode and energy-dispersive X-ray spectroscopy (EDS; Hrstka et al., 2018). A set of intergranular elements was inserted into the numerical models along the boundaries of rock-forming minerals, as shown in Figure 1c. A vertical displacement of 2 mm is directly applied on the upper boundary of the computational model, and a vertical constraint is applied on its bottom boundary. The loading rate of 0.02 mm per step is kept constant during the loading process. The initiation and propagation of microcracks are simulated explicitly using softening of elements, allowing the model to transition from a continuum to discontinuum. During modeling, finite displacements and rotations of the discrete bodies are allowed, while new contacts are recognized. A time step of 5×10^{-4} ms is chosen to ensure the numerical stability for the explicit time integration scheme.

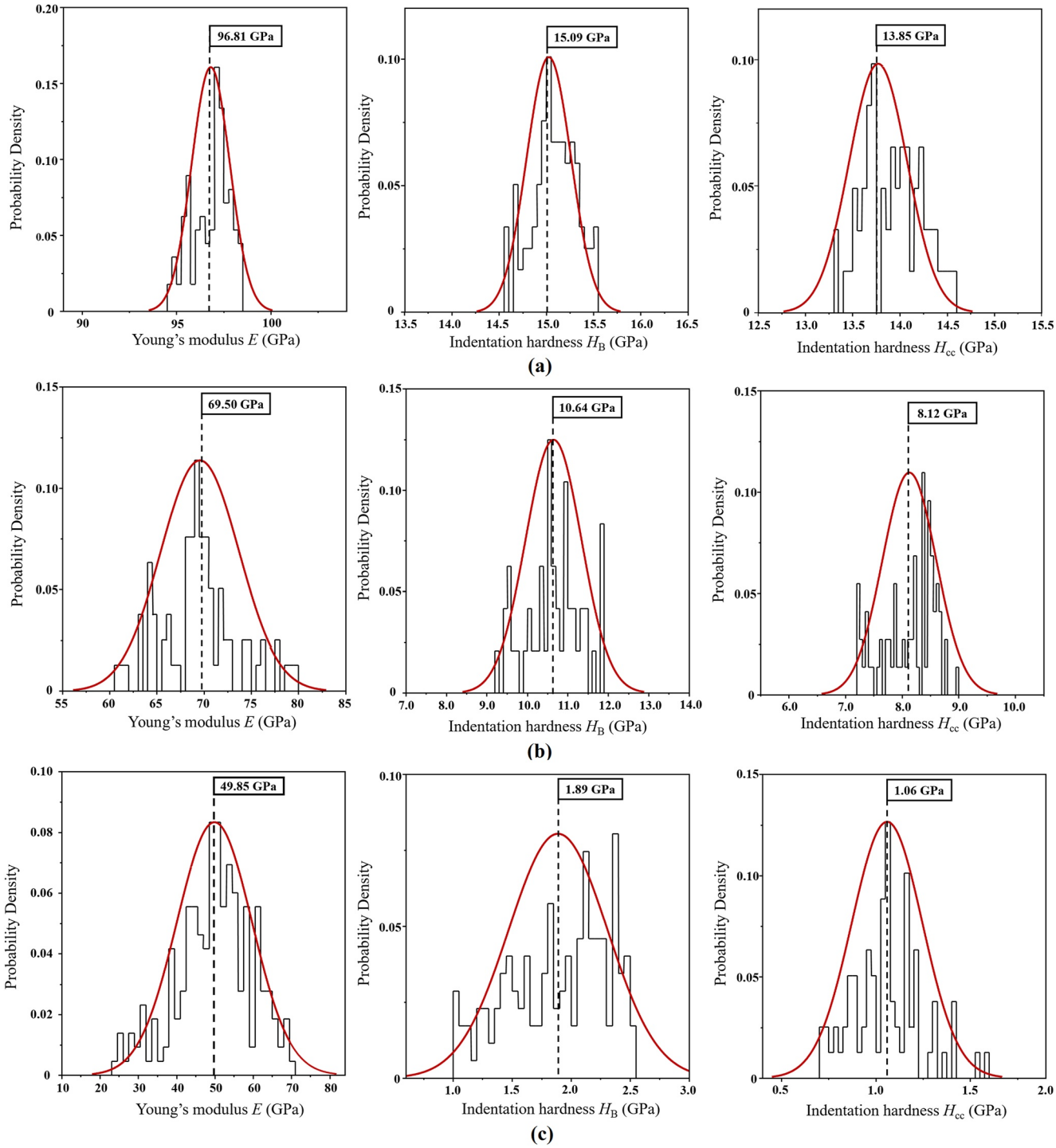


Figure 2. Frequency plots of grid indentation on (a) quartz, (b) feldspar, and (c) biotite, which are fitted with the probability density function to obtain the deconvolution value of Young's modulus E, hardness of the Berkovich indenter H_B, and hardness of the cube-corner indenter H_{CC}.

2.3. Mechanical Properties of Rock-Forming Minerals in AGBM

Nanoindentation testing was performed on a Hysitron TI950 TriboIndenter system. A Berkovich indenter and cube-corner indenter were used for each mineral, setting the same loading parameters. The indentation grids for the two indenters both consist of 100 indentations. The experimental results for the Berkovich indenter and cube-corner indenter of the three minerals are represented in Figure 2. The experimental frequency plots of the

Table 1
Mechanical Properties of Minerals Achieved by Nanoindentation Tests

Mineral	Young's modulus (GPa)	Hardness of Berkovich indenter (GPa)	Hardness of cube-corner indenter (GPa)	c (MPa)	φ (°)
Quartz	96.81	15.09	13.85	1,892	9
Feldspar	69.50	10.64	8.12	606	21
Biotite	49.85	1.89	1.06	16	45

elastic modulus and hardness were fitted by probability density functions. The frictional angle of minerals could be calculated according to the function of friction angle and the ratio of different hardness values measured by the two indenters with different apex angles (Equation 4). Therefore, the cohesion could be determined based on the hardness-to-cohesion relation. The mechanical properties of different minerals are tabulated in Table 1.

The values of other microscale parameters of rock-forming minerals, including density, Poisson's ratio, and tensile strength, were chosen according to the mineral properties suggested in the literature (Bass, 1995; Yu et al., 2015). A literature survey of the thermal expansion coefficients of minerals is presented in Table 2. The numerical simulation calibration results use various values, while the laboratory test results vary because the test samples are different. In addition, there is a lack of experimental data for biotite and feldspar. The thermal expansion coefficients of minerals used in this study were selected from the references and were determined by calibrating the numerical simulation with real-time heating experimental results.

2.4. Mechanical Properties of Interphases Between Different Minerals in AGBM

The AFM (Dimension Icon) was used to measure the geometry and mechanical properties of the interphases between different minerals. The Young's modulus of the interphase was characterized at the microscale by AFM in Tang et al. (2022) to provide a modeling parameter. To date, experimental data on the failure properties of interphases are quite limited. To ensure the accuracy of the microparameters, they were calibrated to match the macroscale properties of the Bukit Timah granite tested in the laboratory.

The failure criterion of intergranular elements was defined by the cohesion c and the angle of internal friction φ, which were calibrated by trial calculation of the stress–strain curve until the numerical and experimental results (Wong & Maruvanchery, 2016) are close in terms of elastic modulus and the UCS. The calibration results are presented in Figure 3. The microparameters listed in Table 3 were proven capable of modeling the strength and microcracking processes of Bukit Timah granite using AGBM.

3. Thermally Induced Microcrack Evolution Process

3.1. Heating Platform

An ultrahigh-temperature heating platform (HS1400G, Instec, Britain) on the optical microscope (BX51M, Olympus, Japan) was developed to observe the microcrack propagation of thin-section samples during heating in real time (see Figure 4a). The high-temperature heating platform is composed of a heating platform, controller, and circulating water cooling pump. Nitrogen was injected into the airtight cavity of the heating platform as vacuum protection gas. The liquid cooling method was used to control the cooling rate of the heating platform. The maximum design temperature of the ultrahigh-temperature heating platform is 1400°C, and the heating accuracy is 0.1°C.

Table 2
Thermal Expansion Coefficient of Minerals Used in the Literature for Numerical Modeling

References	Quartz (10^{-6} K^{-1})	Biotite (10^{-6} K^{-1})	Feldspar (10^{-6} K^{-1})		
			Plagioclase	K-feldspar	Albite
Fei (1995), Z. J. Wu et al. (2020), and Z. H. Zhao (2016)	24.3	3.0	14.1	8.7	–
Z. H. Li et al. (2020)		–	15.4	8.9	–
Badulla et al. (2018)	9–14	12–16.5		4.5	
Siegesmund et al. (2008)	37	35.2	10.4–14.0	12.6–15.8	6.59
Vázquez et al. (2015)	14	16.5		4.5	
Yu et al. (2015)	11	3		6	
F. Wang et al. (2020)	11.5	13.3		5	

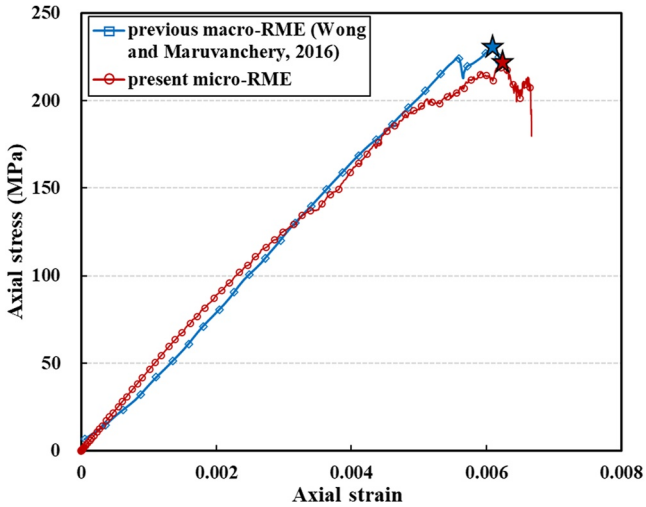


Figure 3. Comparison between the stress–strain curves obtained by the macroscale rock mechanics experiments (macro-RME) (blue line) and microscale rock mechanics experiments (micro-RME)-based model (red line).

3.1.1. Sample Preparation

Singapore Bukit Timah granite rock cores were examined in this study (see Figure 4b). The granite rock is widespread and one of the major rock formations in Singapore. Many researchers have studied its mechanical properties (Z. H. Li et al., 2017, 2020; Wong & Maruvanchery, 2016). It shows significant mechanical deterioration under the influence of heat. The rock sample was prepared as doubly polished thin sections of approximately 60 μm in thickness for petrographic analysis and microthermometric observation. Before the experiment, the slide was heated with an alcohol lamp to dissolve the resin, and the thin-slice sample was removed and immersed in acetone to wash the surface glue to avoid affecting the observation. Then, the samples with existing microcracks were excluded.

3.1.2. The Setup of the Heating Temperature

The sample was heated according to the temperature–time curve represented in Figure 4c as follows: heat from room temperature (25°C) to 100°C at a rate of 20°C/min; maintain the temperature for 5 min, as the thin-section sample is sufficiently small to generate a homogeneous thermal field quickly; heat to 100°C, 200°C, 300°C, 400°C, 500°C, 600°C, 700°C, 800°C, and 900°C successively; finally, reduce the temperature to room temperature at a cooling rate of 20°C/min from the maximum temperature.

3.2. Microstructure Characterization

To analyze the influence of compositional distribution on the temperature-dependent mechanical behavior of Bukit Timah granite, a comprehensive microstructural analysis was performed to identify the mineralogical structure. Thin sections of samples were studied by SEM (Zeiss SIGMA) at Wuhan University Testing Center. BSE images taken at low magnifications clearly show different mineral assemblages and grain boundaries (see Figure 5a). EDS (Oxford UltimMax 40) was used to further determine the chemical components of minerals with different gray values. Figure 5b represents the mineral distribution of the selected zone (detailed descriptions of element distribution and mineral identification are given in Appendix A). Other contents, such as chlorite and calcite, account for minor percentages and have little influence on the overall thermal and mechanical responses of the granite specimen. Therefore, this study does not consider the presence of minor minerals.

3.3. Evolution Process of Microcracks Under Thermal Treatment

The experimental results are shown in Figure 6. The heating of granite up to 300°C did not cause any significant thermally induced microcracks, and almost all grain boundaries remained intact. The quartz crystal exhibits obvious thermal expansion. Thermal cracks can be observed by the naked eye for the samples after thermal treatments at a temperature above 300°C. At 500°C, the lengths of fractures increase substantially, the microfractures propagate and generate further, and some coalesce into larger fractures. At 600°C, microcracks propagated across most grains with an obvious increase in crack width, forming a microcrack network. Meanwhile, the quartz grains are broken into different parts. From 700°C to 800°C, biotite sheets opened along the cleavage planes due

Table 3
Material Parameters Used in Accurate Grain-Based Models

Mineral	Density (kg/m^3)	E (GPa)	Poisson ratio	c (MPa)	φ (°)	Thermal expansion coefficient (10^{-6} K^{-1})	Tensile strength (MPa)
Quartz	2,650	96.81	0.08	1,891	9	24.3	47
Feldspar	2,600	69.50	0.27	606	21	8.9	33
Biotite	2,850	46.41	0.25	16	45	3	25
Interphase	2,650	24.48	0.23	40	50	–	10

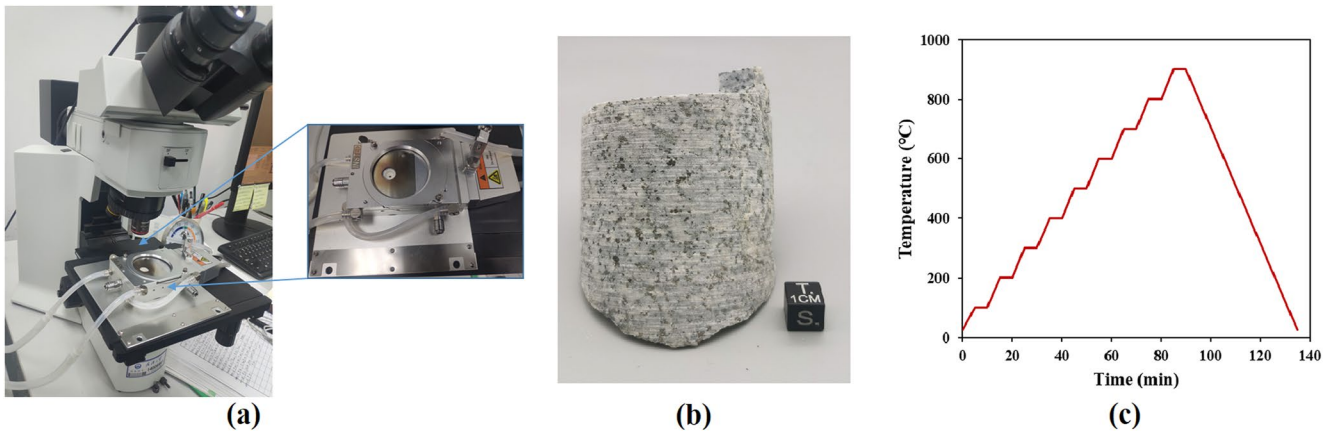


Figure 4. (a) Optical microscope with ultrahigh-temperature heating platform, (b) sample, and (c) experimental procedures.

to expansion, which resulted in basal cleavage being more noticeable in the heated sample. There is macrocrack transgranular failure in biotite. Almost all thermally induced microcracks tend to form during the heating phase rather than during the cooling phase.

3.3.1. The Length Evolution of Microcracks

In Figure 7, the microcracks are highlighted using red lines to observe the failure pattern and quantify the extent of microcracking. Then, the length of microcracks was calculated, and the relationship between microcrack length and heating temperature is plotted in Figure 8. Many published references have demonstrated that thermal fracturing in rock often starts from a threshold temperature (Geraud et al., 1992; Inserra et al., 2013). The temperature of 300°C may be considered a threshold temperature of granite for thermal microcracking according to the curve of microcrack length evolution with temperature. In addition, the number of microcracks increases with increasing of heating temperature between 500°C and 600°C. The microcracks observed in granite include intergranular microcracks and intragranular microcracks. The crack count evolution of different types of microcracks during temperature loading is shown in Figure 8b. Both types of microcracks gradually increase in number in response to loading. Intergranular cracks are more frequent at quartz–feldspar interfaces than at quartz–biotite or feldspar–biotite interfaces. Due to the interaction with quartz, the number of microcracks in feldspar also increases rapidly between the heating temperatures of 500°C–600°C.

3.3.2. Intergranular and Intragranular Microcracks

The microcracks and grain distribution with different heating temperatures are shown in Figure 9. There is clear mineralogical assembly in the granite specimens, mainly with quartz, feldspar, and biotite. When the heating

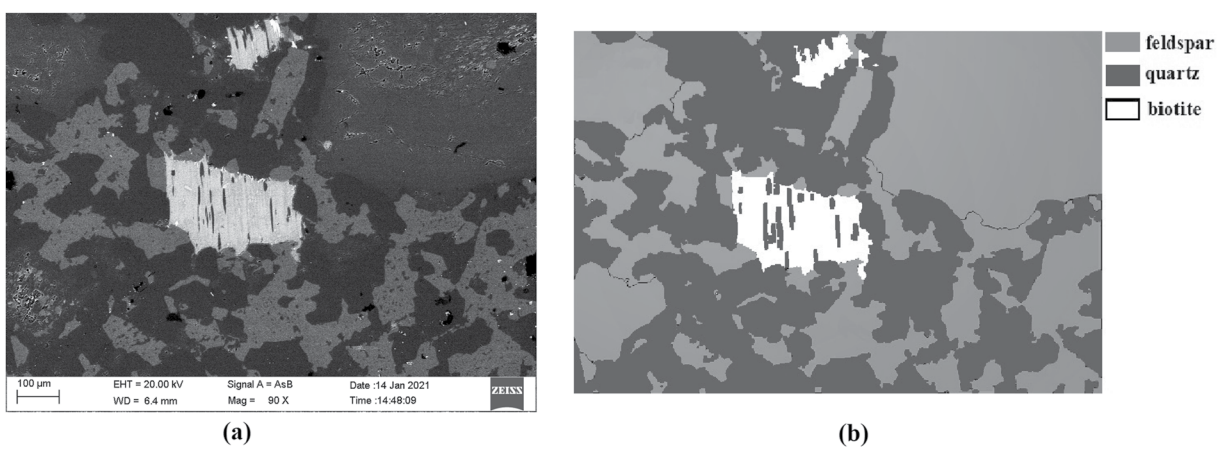


Figure 5. Based on the (a) backscattered electron (BSE) images, (b) energy-dispersive X-ray spectroscopy (EDS)-layered image, the distribution of different minerals and the microstructure can be identified and characterized.

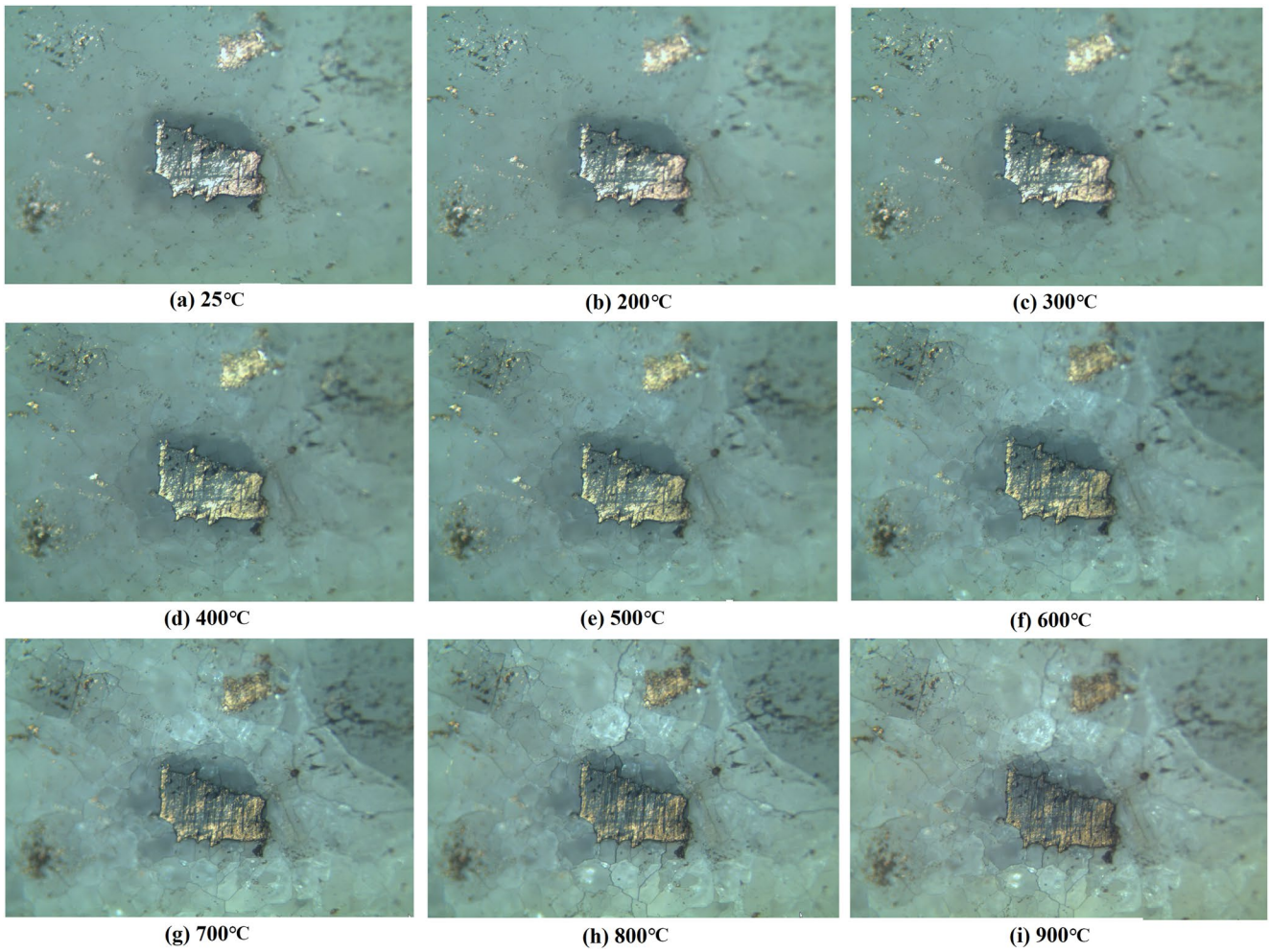


Figure 6. Microscopy images of the real-time experiment exhibiting the microcrack evolution of the granite sample at different temperatures: obvious microcracks can be observed after 300°C; then, the microcracks propagate and coalesce between 400°C and 600°C; at 800°C–900°C, the sample is almost completely broken.

temperature was over 400°C, there were many discontinuous microcracks in the boundary between feldspar and quartz. Between the heating temperatures of 500°C and 600°C, the microcracks between feldspar and quartz substantially propagated, and some coalesced into larger cracks. Due to the interaction between biotite and quartz, the intergranular microcracks between the biotite and quartz also increase. The microcracks in feldspar develop rapidly through sericitized areas, inclusions, and cleavage planes. At 600°C, with the temperature increasing further, microfractures are almost completely encircling the quartz grain. Meanwhile, microcracks connect the boundary cracks between biotite and quartz with intragranular cracks in quartz, forming rings macrocracks around biotite. Between the heating temperatures of 700°C and 800°C, the number of intragranular microcracks in biotite increases rapidly, which is obviously influenced by the preserved cleavage planes. The boundary and intragranular cracks propagate and coalesce throughout the entire granite when the temperature is above 800°C.

3.4. Investigating the Microcracking With AGBM

3.4.1. Numerical Models

An AGBM has been applied to understand the evolution of thermal stresses and the internal mechanism of microcracking in polymineralic rocks. According to the real-time observation area of the heating instrument, a numerical model with an actual size of 1.2 × 0.875 mm was constructed, which contained a total of 270,060 elements (643 × 420). After the finite element mesh was created, the mechanical properties and thermophysical properties of minerals were assigned to the elements based on the mineral distribution. Considering that the observed area

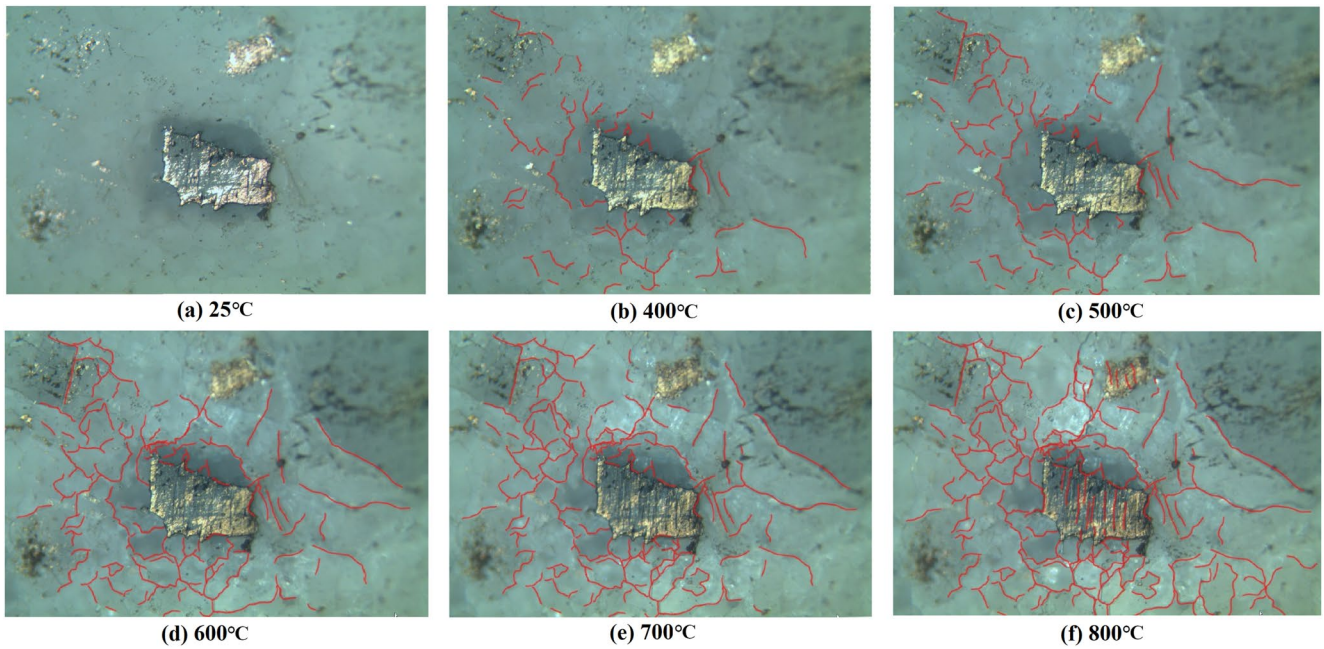


Figure 7. Red lines are overlaid on the observed microcracks in the microscopic images of the specimen to enhance visibility and count the length of the microcracks.

in the thermal experiments is only a part of the sample, the simulated model is subjected to the stress of the surrounding minerals. Rock materials are added around the model to simulate the real experimental state as much as possible, which adopts the physical and mechanical properties of feldspar minerals to characterize the average properties of granite. The thermal loading process was from room temperature to 900°C. During simulation, the heat stress state of each element is solved. When the strain state of elements satisfies the Mohr-Coulomb criterion with tension cutoff, microcracks are produced by deleting completely damaged elements so that tensile or shear damage occurs. Macroscopic cracks may form where these microcracks propagate and coalesce.

3.4.2. Numerical Results and Discussion

The results of numerical modeling indicate that thermal stresses that lead to microcracking significantly depend on the mineralogy. Microcracks in granite are induced by the heterogeneity of thermal expansion coefficients and mechanical properties between different minerals during the heating process. As shown in the Von-Mises stress diagram (Figure 10a), when the sample is heated, quartz withstands much more

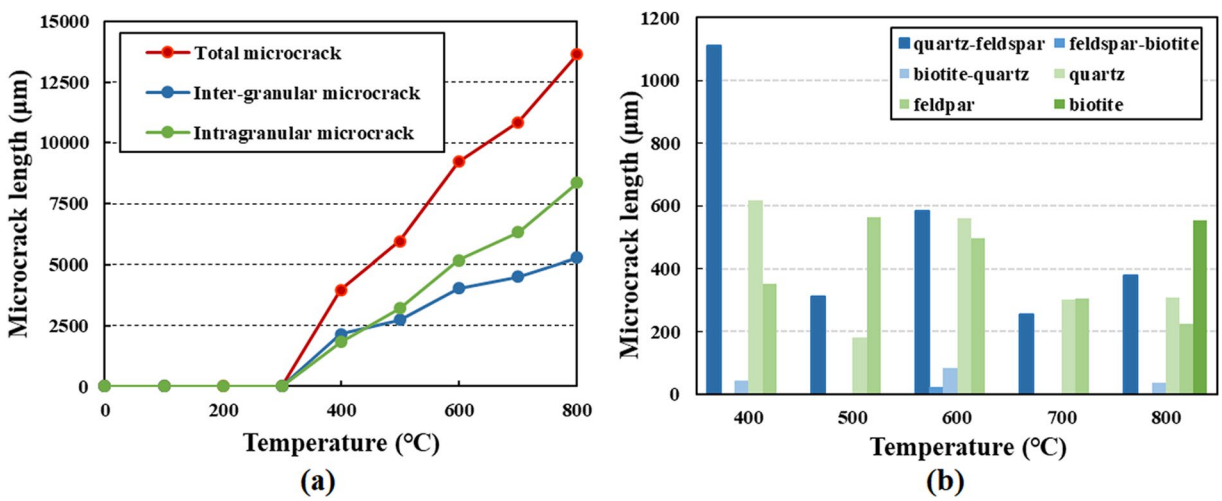


Figure 8. Microcrack length versus temperature during heating of a granite sample.

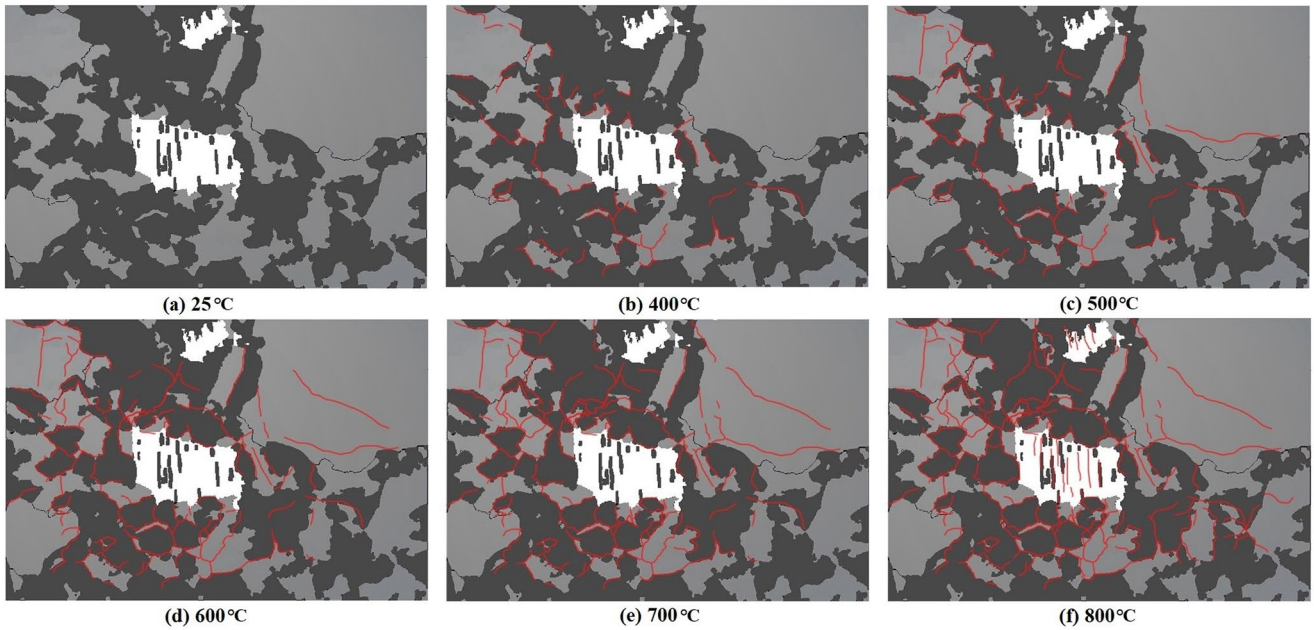


Figure 9. Distribution characteristics of microcracks between minerals: microcracks initiate from the feldspar–quartz boundaries. There are many intragranular microcracks in feldspar. Intergranular and intragranular microcracks substantially propagate and separate quartz into different polygons. The intragranular cracks in biotite develop along the cleavage plane.

thermal stress than the other two minerals. With increasing temperature, the stresses of the granite sample accumulate further. Quartz experiences the greatest internal compressive stress due to its maximum thermal expansion coefficient (see Figures 11a and 11b). Meanwhile, uneven tensile and compressive stresses are produced at the boundaries between quartz and biotite, which ultimately results in the formation of microcracks. Figure 11c shows that shear stress concentration occurs in the interface area between quartz and feldspar, especially along bottlenecks of quartz between feldspar grains. The existence of high shear stress concentrations in quartz around biotite explains the formation of connected microcracks at the corresponding locations found in microscopic observations. Previous studies also confirmed that high maximum principal stress concentrated along the crystal boundaries forms the network and that there was a spectacular increase in maximum principal stress during heating when biotite is considered in the structure (Vázquez et al., 2015; Yu et al., 2015).

Microcracks appeared in the numerical model at 300°C, which appeared at the boundary of biotite and spread along interfaces between the quartz and feldspar grains. Microscale experiments also showed that microcracks propagate from biotite boundaries toward other minerals. With the temperature increasing to 600°C, the number of failed elements increases quickly, forming microcrack networks along the grain boundaries. The simulated thermal cracking phenomena are consistent with the laboratory test results, which demonstrates that the proposed model can not only simulate thermal cracking but also reveal the mechanism of thermal cracking. The distribution of intergranular thermal stress during a uniform temperature change is related to the crystal heterogeneity of granite. Specifically, the thermal behavior of rock depends not only on the microstructure but also on the proportion, size, texture, elastic modulus, and thermal expansion coefficient of minerals.

Although numerical simulation is able to explain the thermal stress evolution of granite accurately, it is difficult to reproduce most of the intragranular cracks observed during the experiment. The preferential paths for crack growth in feldspar may be along the previously formed cracks generated during the tectonic history of the rock (Undul et al., 2015). Additionally, the alteration of feldspar minerals and twinning planes also influences the propagation of intragranular cracks. Meanwhile, quartz grains are also prone to intragranular cracks because of their polycrystalline microstructure. Therefore, it is necessary to consider the anisotropy and crystallographic orientations of minerals in numerical models, which may be beneficial to account for the preferred pathways that fractures tend to propagate along weak planes within the crystals (Zhong et al., 2014).

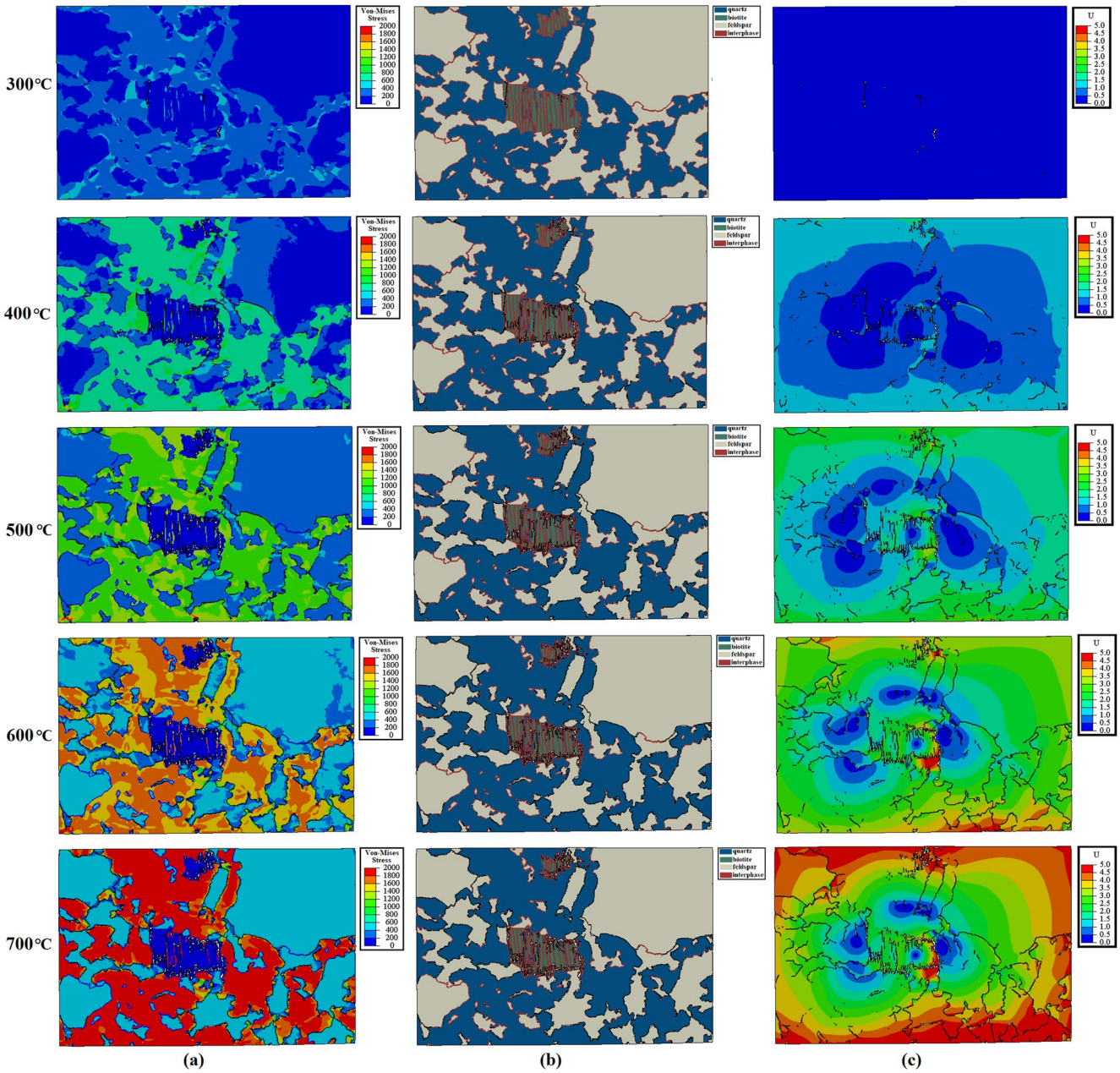


Figure 10. The evolution of (a) von-Mises stress, (b) microcracks, and (c) displacement in the granite sample at different temperatures.

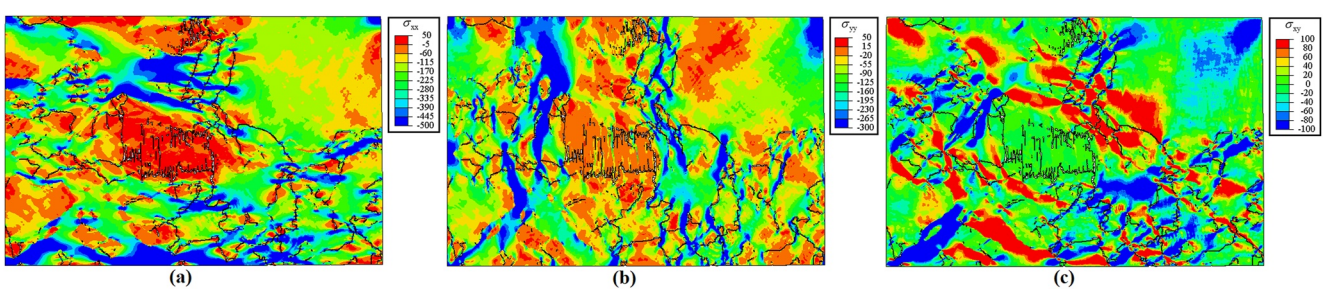


Figure 11. Simulated results of (a) horizontal stress σ_{xx}, (b) vertical stress σ_{yy}, and (c) shear stress σ_{xy} at 500°C (unit: MPa).

4. Effect of Temperature on the Mechanical Properties of Granite

4.1. Microcracking Behavior

The numerical model established based on the mesostructure of granite samples in Section 2.2 was heated at temperatures ranging from 25°C to 900°C with free boundary conditions to simulate the thermally induced cracking process of intact granite cores. The numerical simulation results show the evolution of the stress and displacement of granite after heating. As illustrated in Figure 12, isolated microcracks initiate at 300°C when the stresses induced within some elements first meet the stress criterion. When the temperature is elevated to 400°C, and the damage occurs mainly distributed at the biotite and feldspar–quartz boundary in the center of the granite sample due to stress concentrations. After the temperature reaches 500°C, microcrack networks are formed due to the coalescence of microcracks initiated around mineral grains and intragranular cracks within weak mineral grains. With increasing temperature, thermal cracks are fully spread within the numerical specimen, the cracks propagating along grain boundaries are nearly closed, and many polygonal cracks are formed around the mineral grains. This phenomenon has also been reported in other published references (Vázquez et al., 2015; Yu et al., 2015).

4.2. Stress–Strain Response

To study the effect of temperature on the macromechanical behavior of granite, a series of uniaxial compressive tests was conducted at different temperatures from room temperature to 900°C. The loading process applied axial external displacement to the numerical specimen heated to a specific temperature until the numerical specimen completely lost its loadbearing capability. The stress–strain curves of the uniaxial compressive tests are plotted in Figure 13a. There are two main methods to characterize the Young's modulus based on stress–strain curves, including tangent Young's modulus and secant Young's modulus (Jaeger et al., 2007). The secant Young's modulus, which is defined to be the ratio of the peak stress to the peak strain, was used in the present work. The rock specimens below 500°C exhibited a similar failure mode: (a) the elastic stage where the stress–strain curve was approximately linear and peak stress was eventually reached and (b) the softening stage where the stress–strain curve declined steeply and the rock specimen fractured rapidly. However, it is evident that the slopes of the stress–strain curves, as well as the peak stresses, decreased with increasing temperature. The thermal-stress-induced fracture damage in crystalline rocks resulted in a decrease in UCS and Young's modulus. The UCS and Young's modulus as a function of temperature are shown in Figure 13b. When the heating temperature reaches the crack initiation threshold (300°C), the progressive development of cracks induced the extension of the microcrack network and created irreversible deformations in the granite. Moreover, beyond 500°C, the collapse and weakening of the bridge minerals increase the crack density and size, resulting in the progressive accumulation of plastic strain and the decline in the brittle properties of granite. A flat peak was observed for the stress–strain curve at a temperature of 500°C, which indicates that higher temperatures generally encourage ductility (Z. H. Zhao, 2016).

5. Discussion

In recent decades, many laboratory macroscale experiments have investigated the influence of heating on the mechanical properties of granite, which show similar mechanical property evolution with temperature despite differences in the mineral content and grain size. Table 4 summarizes the experimental results of the variation of UCS, Young's modulus, and peak strain of granite with temperature in the extensive literature. The evolutions of the normalized UCS, Young's modulus, and peak strain are shown in Figure 14. Overall, as the heating temperature increases, the UCS and Young's modulus show a deceasing trend: (a) when the heating temperature is below 400°C, the decreasing trend of the strength is not obvious, and some experimental data show a slight fluctuating upward trend. (b) From 400°C to 600°C, the peak strength decreases rapidly and linearly. Compared with the UCS and Young's modulus, the variation trends of the peak strain with heating temperature are almost opposite, showing an increasing trend. The change in peak strain of the heated granite rocks can also be divided into two stages along the heating temperatures. Once the temperature reaches 400°C, the peak strain displays a notable increasing trend. The threshold temperature range of the mechanical properties of granite varies with temperature from 400°C to 600°C.

In the present research, the combinations of microscopic observations and the results of numerical modeling show the thermal damage mechanism for granite: (a) at low temperature, thermal expansion of mineral grains dominates the mechanical response. (b) In the range of 300°C–600°C, the intergranular and intragranular microcracks

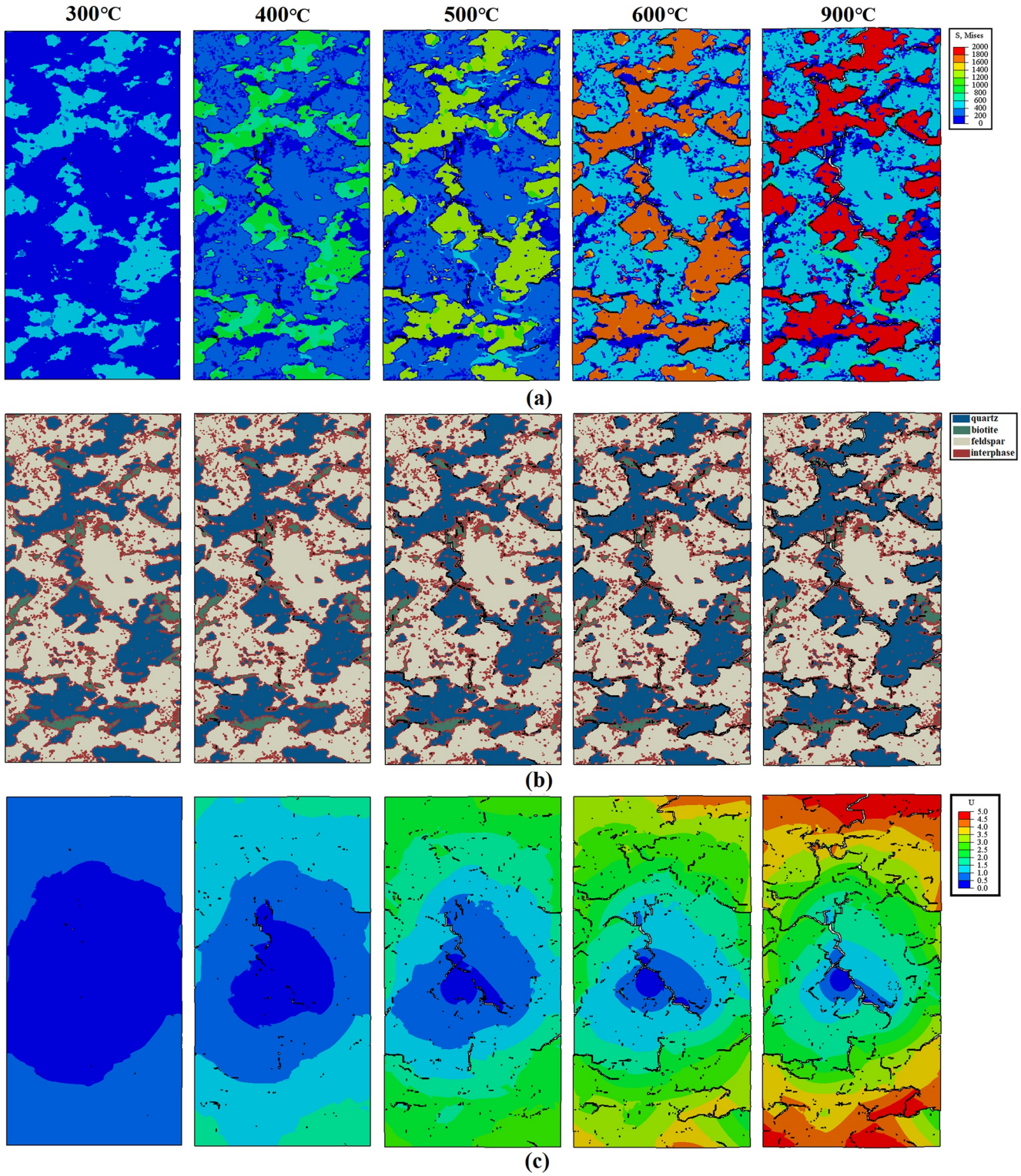


Figure 12. The evolution of (a) thermal stress, (b) microcracks, and (c) displacement of granites subjected to thermal loading.

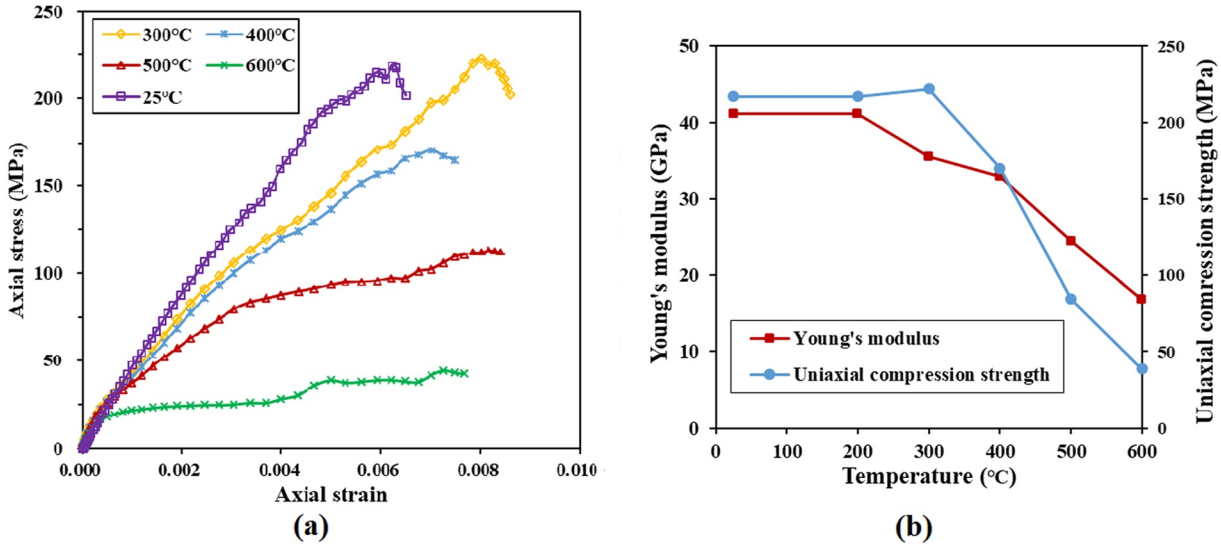


Figure 13. Variation of the (a) stress–strain curve, (b) Young's modulus and uniaxial compressive strength of granite at different temperatures.

initiate, propagate, and finally coalesce. In addition, the results of permeability (Zhang et al., 2016), wave velocity (Z. L. Shao et al., 2020), and porosity tests (Lin, 2002; F. B. Wu et al., 2021) in many studies have indirectly confirmed this phenomenon: fluid permeability, porosity, and electrical conductivity show increases associated with the form of a well-interconnected microcrack network (Glover et al., 1995). The curves of total microcracks obtained in real-time heating tests with temperatures and the evolution of macroscale mechanical behavior are compared in Figure 14. Therefore, the generation of microcracks induced by heating is the main reason for the deterioration of the compressive and tensile strengths of granite and the increase in plastic deformation. The increase in microcracks may be related to the structural changes in mineral composition caused by internal moisture continuously escaping from the rock with increasing temperature, especially when the temperature reaches approximately 300°C, at which point the strong bonding water will escape (Zhang et al., 2016). The α–β quartz transition at 573°C was noticed as an important factor generating crystalline deformation in rocks (Chaki et al., 2008), which can be manifested as significant volumetric expansion. While the phase transition temperature is not the threshold of crack initiation, the dominant impact of the phase transition is the widening of preexisting microcracks rather than the formation of new microcracks (F. Wang et al., 2020).

Table 4
Summary of Macroexperimental Results on the Influence of Thermal Loading on the Mechanical Properties of Granite

Heating temperature (°C)	Uniaxial compressive strength	Elastic modulus	Peak strain	Critical temperature (°C)	References
30–600	Increase–decrease	Increase–decrease	–	400–500	Homand-Etienne and Houpert (1989)
20–1000	Decrease	Increase–decrease	Increase	400–600	Chen et al. (2012)
23–1000	Decrease generally	Increase–decrease	Decrease–increase	400–600	S. S. Shao et al. (2015)
25–900	Decrease generally	Decrease generally	Increase	450	Huang et al. (2017)
20–600	Decrease	Decrease generally	Increase	200	Y. S. Zhao et al. (2017)
20–800	Increase–decrease	Decrease	Increase generally	300	Kumari, Ranjith, Perera, Chen, et al. (2017)
25–1000	Decrease generally	Decrease generally	Increase generally	300	Badulla et al. (2018)
25–800	Increase–decrease	Increase–decrease	Increase generally	500	Z. L. Shao et al. (2020)
25–1000	Decrease	Decrease	Increase generally	400	X. L. Xu and Karakus (2018)
25–800	Decrease generally	Decrease generally	Increase generally	400	Miao et al. (2021)
25–600	Decrease	Decrease generally	Increase	400–500	Sha et al. (2020)
25–1000	Increase–decrease	Increase–decrease	Increase–decrease	400	F. Wang et al. (2020)

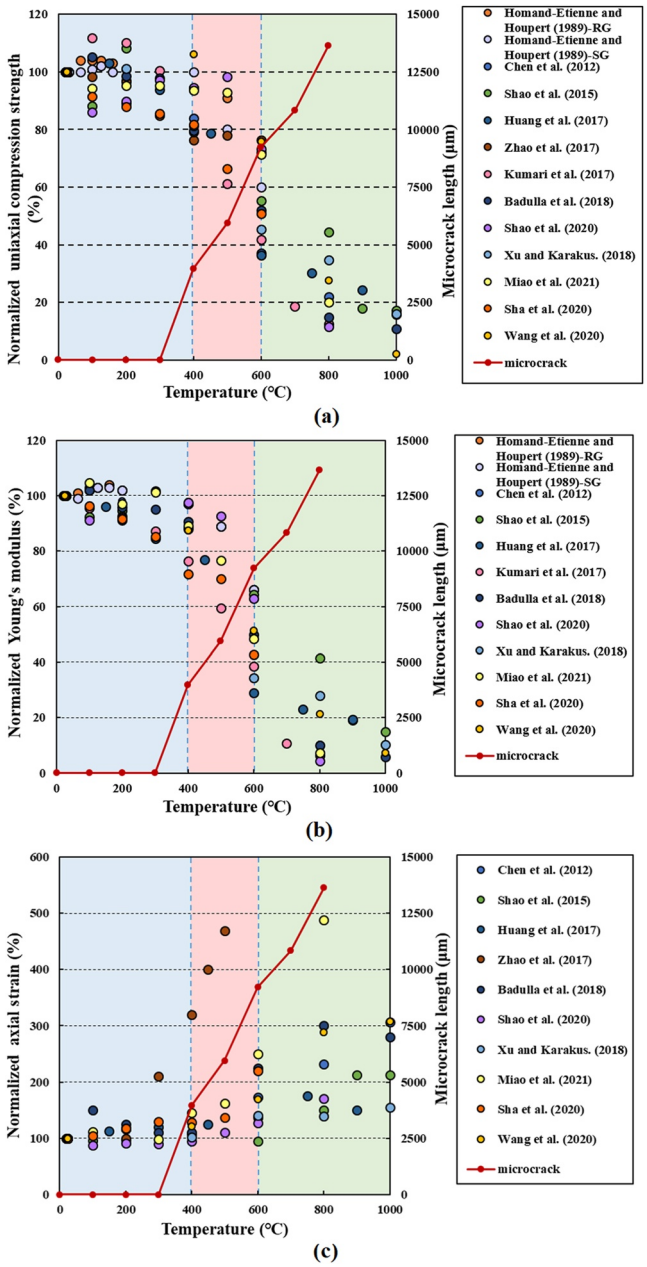


Figure 14. The comparison of total microcracks curve obtained in real-time heating test and the variation of the (a) uniaxial compressive strength, (b) Young's modulus, and (c) axial strain versus temperature in the literature.

It is noticed that, the present work focuses on the effect of thermal loading, however ignored the influence of confining stress which widely exist in deep reservoirs. Currently, it is still challenge to experimentally visualize microcracking and investigate the coupling effect of thermal loading and confining stress on the mechanical behavior of rocks at multiscale. Some researchers proposed alternative to understand the coupling effect of thermal loading and confining stress. Y. S. Zhao et al. (2017) have developed a triaxial compression experiment system with constant horizontal confining stress is 25 MPa, which is able to apply high-temperature loading and confining stress simultaneously. They pointed out that, the overall decreasing trend of macroscale Young's modulus of granites is consistent with that of unconfined stress, although the macroscale Young's modulus is enhanced due to confining stress. Because of technical limitation, more researchers only investigated the influence of thermal loading or investigate the mechanical properties after heating treatment (Yang et al., 2020). Additionally, the high-pressure, high-temperature gas deformation apparatus is also widely used to investigate the coupling effect of thermal loading and confining stress (Vandermoledn, 1981). The increases in porosity are found to be ~2.0%, ~1.6%, ~1.0%, and ~0.6%, respectively, for 1 atm, 100, 200, and 300 MPa between 200°C and 840°C. Opening of cracks is increasingly suppressed at higher confining pressures. The observed trend indicates that differential thermal expansion can no longer cause crack opening in dry granite at confining pressures in excess of 450 MPa (Vandermoledn, 1981). Nevertheless, this kind of experimental research mainly focuses on the mechanism of quartz phase transition and thermal expansion. Overall, the existing experimental techniques are not possible to visualize microcracking process and generate the relationship between grain scale and macroscale. In future work, it is necessary to polish the present experiment system to consider the coupling effect of thermal loading and confining stress.

6. Conclusion

In this study, the microcrack evolution of granite subjected to heating loading was first observed in real time and in situ with a heating table and microscope. An AGBM was developed and applied for investigating the thermal cracking process numerically, in which the micro-RME were used to characterize the morphology and mechanical properties of minerals. On the basis of the experiments and numerical results, the mechanism of thermal-induced microcracks and the effect of temperature on the mechanical properties of granite were discussed. The following conclusions can be drawn:

1. The laboratory test shows that microcracks initiate at 300°C and these microcracks coalesce in the temperature range of 400°C–600°C. The threshold temperature of microcracks initiation is much earlier than the α–β quartz transition temperature (573°C). The thermally induced microcracks initially develop along the quartz–feldspar boundaries. Intragranular microcracks occur in feldspar in a high proportion, and microcracks inside biotite obviously propagate along the preserved cleavage planes.
2. A great number of references show that, the decreasing trend of the macroscale strength of granites is not obvious when the heating temperature is below 400°C, however the macroscale strength decreases rapidly and linearly from 400°C to 600°C. The present experimental results show that the coalescence of microcracks appears between 400°C and 600°C, which mainly contributes to the drop in macroscale properties. Additionally, the simulation of uniaxial compression tests of granite after thermal loading confirmed that microcrack accumulation can significantly reduce the UCS and Young's modulus of granites. Granite can still maintain

brittle failure characteristics at lower temperatures, and the samples above 500°C obviously show ductile failure behavior.

3. Accurate grain-based modeling is able to reproduce the propagation of thermally induced microcracks in granite samples by incorporating geometric features and accurate mechanical parameters of minerals. It was revealed that the differential thermal expansions and mechanical deformations caused by rock heterogeneity altered the thermal stress distribution, creating local tensile stresses between feldspar and quartz and shear concentrations around biotite.

Appendix A

The major elements of granite sample are shown in different colors in the EDS images, where the bright color images indicate higher concentrations (higher energy dispersion). Figures A1a–A1d show the elemental distributions of Si, Al, Mg, and Fe based on the EDS-layered images. The highlighted areas in purple are Si-rich grained minerals. These areas also show the absence of Al and are thus identified as quartz. The regions where the blue S element and green Fe element overlap can be recognized as biotite. The Si-rich region excluding the region identified as biotite is feldspar.

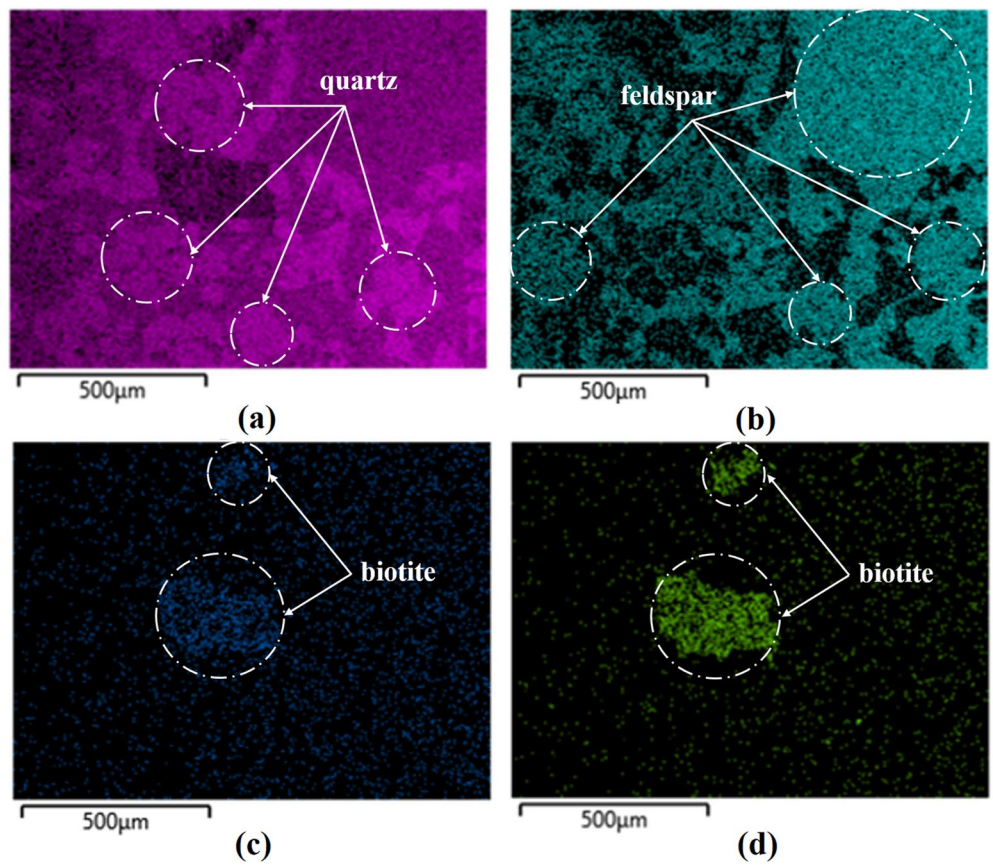


Figure A1. Different minerals can be identified based on the energy-dispersive X-ray spectroscopy (EDS) element mapping of (a) Si, (b) Al, (c) Mg, and (d) Fe.

Data Availability Statement

Data sets of nanoindentation and image sets of heating experiments related to this article are made available from a public repository of research data, Zenodo, through the following link, https://zenodo.org/record/6620015# and https://zenodo.org/record/7219920#, respectively.

Acknowledgments
The work was supported by the National Natural Science Foundation of China (Grants 12172264 and 41941018), Basic Research Program of Central Government Funds for Shenzhen Science and Technology Development (2021Szvup103) and Shenzhen Fundamental Research Program (JCYJ20220530140602005).

References

Aghahosseini, A., & Breyer, C. (2020). From hot rock to useful energy: A global estimate of enhanced geothermal systems potential. *Applied Energy*, *279*, 115769. https://doi.org/10.1016/j.apenergy.2020.115769

An, M. K., Zhang, F. S., Min, K. B., Elsworth, D., He, C. R., & Zhao, L. X. (2022). Frictional stability of metamorphic epidote in granitoid faults under hydrothermal conditions and implications for injection-induced seismicity. *Journal of Geophysical Research: Solid Earth*, *127*, e2021JB023136. https://doi.org/10.1029/2021JB023136

An, M. K., Zhang, F. S., Min, K. B., Elsworth, D., Marone, C., & He, C. R. (2021). The potential for low-grade metamorphism to facilitate fault instability in a geothermal reservoir. *Geophysical Research Letters*, *48*, e2021GL093552. https://doi.org/10.1029/2021GL093552

Badulla, L. A. I., Ranjith, G. P., Tharaka, R. D., Mandadige, A. S., Dornadula, D., & Wanniarachchige, K. G. P. (2018). An influence of thermally-induced micro-cracking under cooling treatments: Mechanical characteristics of Australian granite. *Energies*, *11*(6), 1338. https://doi.org/10.3390/en11061338

Bass, D. (1995). Elasticity of minerals, glasses, and melts. In T. J. Ahrens (Ed.), *Mineral physics and crystallography: A handbook of physical constants* (Vol. 2, pp. 45–63). American Geophysical Union.

Chaki, S., Takarli, M., & Agbodjan, W. P. (2008). Influence of thermal damage on physical properties of a granite rock: Porosity, permeability and ultrasonic wave evolutions. *Construction and Building Materials*, *22*(7), 1456–1461. https://doi.org/10.1016/j.conbuildmat.2007.04.002

Chen, Y. L., Ni, J., Shao, W., & Azzam, R. (2012). Experimental study on the influence of temperature on the mechanical properties of granite under uni-axial compression and fatigue loading. *International Journal of Rock Mechanics and Mining Sciences*, *56*, 62–66. https://doi.org/10.1016/j.ijrmms.2012.07.026

Du, S. G., Lin, H., Yong, R., & Liu, G. J. (2022). Characterization of joint roughness heterogeneity and its application in representative sample investigations. *Rock Mechanics and Rock Engineering*, *55*(6), 3253–3277. https://doi.org/10.1007/s00603-022-02837-4

Fan, L. F., Gao, J. W., Wu, Z. J., Yang, S. Q., & Ma, G. W. (2018). An investigation of thermal effects on micro-properties of granite by X-ray CT technique. *Applied Thermal Engineering*, *140*, 505–519. https://doi.org/10.1016/j.applthermaleng.2018.05.074

Fan, L. F., Wu, Z. J., Wan, Z., & Gao, J. W. (2017). Experimental investigation of thermal effects on dynamic behavior of granite. *Applied Thermal Engineering*, *125*, 94–103. https://doi.org/10.1016/j.applthermaleng.2017.07.007

Fei, Y. (1995). *Mineral physics and crystallography: A handbook of physical constants*. AGU.

Ganneau, F. P., Constantinides, G., & Ulm, F. J. (2006). Dual-indentation technique for the assessment of strength properties of cohesive-frictional materials. *International Journals of Solids and Structures*, *43*(6), 1727–1745. https://doi.org/10.1016/j.ijsolstr.2005.03.035

Geraud, Y., Mazeolle, F., & Raynaud, S. (1992). Comparison between connected and overall porosity of thermally stressed granites. *Journal of Structural Geology*, *14*(8–9), 981–990. https://doi.org/10.1016/0191-8141(92)90029-V

Glover, P. W., Baud, P., Darot, M., Meredith, P. G., Boon, S. A., LeRavale, M., et al. (1995). α/β phase transition in quartz monitored using acoustic emissions. *Geophysical Journal International*, *120*(3), 775–782. https://doi.org/10.1111/j.1365-246X.1995.tb01852.x

Griffiths, L., Heap, M. J., Baud, P., & Schmittbuhl, J. (2017). Quantification of microcrack characteristics and implications for stiffness and strength of granite. *International Journal of Rock Mechanics and Mining Sciences*, *100*, 138–150. https://doi.org/10.1016/j.ijrmms.2017.10.013

Griffiths, L., Lengliné, O., Heap, M. J., Baud, P., & Schmittbuhl, J. (2018). Thermal cracking in westerly granite monitored using direct wave velocity, coda wave interferometry, and acoustic emissions. *Journal of Geophysical Research: Solid Earth*, *123*, 2246–2261. https://doi.org/10.1002/2017JB015191

Guo, S. C., Dai, Q. L., Sun, X., & Xiao, X. H. (2017). X-ray CT characterization and fracture simulation of ASR damage of glass particles in alkaline solution and mortar. *Theoretical and Applied Fracture Mechanics*, *92*, 76–88. https://doi.org/10.1016/j.tafmec.2017.05.014

Homand-Etienne, F., & Houpert, R. (1989). Thermally induced microcracking in granites: Characterization and analysis. *International Journal of Rock Mechanics and Mining Science & Geomechanics Abstracts*, *2*(26), 125–134. https://doi.org/10.1016/0148-9062(89)90001-6

Hrstka, T., Gottlieb, P., Skála, R., Breiter, K., & Motl, D. (2018). Automated mineralogy and petrology—Applications of TESCAN Integrated Mineral Analyzer (TIMA). *Journal of Geosciences*, *63*(1), 47–63. https://doi.org/10.3190/jgeosci.250

Huang, Y. H., Yang, S. Q., Tian, W. L., Zhao, J., Ma, D., & Zhang, C. S. (2017). Physical and mechanical behavior of granite containing pre-existing holes after high temperature treatment. *Archives of Civil and Mechanical Engineering*, *17*(4), 912–925. https://doi.org/10.1016/j.acme.2017.03.007

Inserra, C., Biwa, S., & Chen, Y. (2013). Influence of thermal damage on linear and nonlinear acoustic properties of granite. *International Journal of Rock Mechanics and Mining Sciences*, *62*, 96–104. https://doi.org/10.1016/j.ijrmms.2013.05.001

Jaeger, J. C., Cook, N. G. W., & Zimmerman, R. W. (2007). *Fundamentals of rock mechanics* (4th ed.). Blackwell.

Jiao, Y. Y., Zhang, X. L., Zhang, H. Q., Li, H. B., Yang, S. Q., & Li, J. C. (2015). A coupled thermo-mechanical discontinuum model for simulating rock cracking induced by temperature stresses. *Computers and Geotechnics*, *67*, 142–149. https://doi.org/10.1016/j.compgeo.2015.03.009

Johnson, S. E., Song, W. J., Cook, A. C., Vel, S. S., & Gerbi, C. C. (2021). The quartz $\alpha \leftrightarrow \beta$ phase transition: Does it drive damage and reaction in continental crust? *Earth and Planetary Science Letters*, *553*, 116622. https://doi.org/10.1016/j.epsl.2020.116622

Kumari, W. G. P., Ranjith, P. G., Perera, M. S. A., Chen, B. K., & Abdulagatov, I. M. (2017). Temperature-dependent mechanical behaviour of Australian Strathbogie granite with different cooling treatments. *Engineering Geology*, *229*, 31–44. https://doi.org/10.1016/j.enggeo.2017.09.012

Kumari, W. G. P., Ranjith, P. G., Perera, M. S. A., Shao, S., Chen, B. K., Lashin, A., et al. (2017). Mechanical behaviour of Australian Strathbogie granite under in-situ stress and temperature conditions: An application to geothermal energy extraction. *Geothermics*, *65*, 44–59. https://doi.org/10.1016/j.geothermics.2016.07.002

Li, Y. C., Luo, S. M., Lu, M., Wu, Y. K., Zhou, N., Wang, D. F., et al. (2021). Cross-scale characterization of sandstones via statistical nanoindentation: Evaluation of data analytics and upscaling models. *Journal of Rock Mechanics and Mining Sciences*, *142*, 104738. https://doi.org/10.1016/j.ijrmms.2021.104738

Li, Z. H., Wong, L. N. Y., & Teh, C. I. (2017). Low cost colorimetry for assessment of fire damage in rock. *Engineering Geology*, *228*, 50–60. https://doi.org/10.1016/j.enggeo.2017.07.006

Li, Z. H., Wong, L. N. Y., & Teh, C. I. (2020). Influence of thermal and mechanical loading on development of microcracks in granite. *Rock Mechanics and Rock Engineering*, *53*(5), 2035–2051. https://doi.org/10.1007/s00603-019-02030-0

Lin, W. R. (2002). Permanent strain of thermal expansion and thermally induced microcracking in Inada granite. *Journal of Geophysical Research*, *107*(B10), 2215. https://doi.org/10.1029/2001JB000648

Liu, S. Y., Zhen, H., & Hu, L. L. (2022). Interfacial microstructure between ultrahigh-performance concrete–normal concrete in fresh-on-fresh casting. *Construction and Building Materials*, *322*, 12674. https://doi.org/10.1016/j.conbuildmat.2022.126476

Liu, Y. W., Liu, A., Liu, S. M., & Kang, Y. (2022). Nano-scale mechanical properties of constituent minerals in shales investigated by combined nanoindentation statistical analyses and SEM–EDS–XRD techniques. *Journal of Rock Mechanics and Mining Sciences*, *159*, 105187. https://doi.org/10.1016/j.ijrmms.2022.105187

Luo, S. M., Lu, Y. H., Wu, Y. K., Song, J. L., DeGroot, D. J., Jin, Y., & Zhang, G. P. (2020). Cross-scale characterization of the elasticity of shales: Statistical nanoindentation and data analytics. *Journal of the Mechanics and Physics of Solids*, *140*, 103945. https://doi.org/10.1016/j.jmps.2020.103945

Marini, L., & Manzella, A. (2005). Possible seismic signature of the α–β quartz transition in the lithosphere of Southern Tuscany (Italy). *Journal of Volcanology and Geothermal Research*, *148*(1–2), 81–97. https://doi.org/10.1016/j.jvolgeores.2005.03.015

Miao, S. T., Pan, P. Z., Zhao, X. G., Shao, C. Y., & Yu, P. Y. (2021). Experimental study on damage and fracture characteristics of Beishan granite subjected to high-temperature treatment with DIC and ae techniques. *Rock Mechanics and Rock Engineering*, *54*(2), 721–743. https://doi.org/10.1007/s00603-020-02271-4

Nasseri, M. H. B., Tatone, B. S. A., Grasselli, G., & Young, R. P. (2009). Fracture toughness and fracture roughness interrelationship in thermally treated westerly granite. *Pure and Applied Geophysics*, *166*(5–7), 801–822. https://doi.org/10.1007/s00024-009-0476-3

Nicco, M., Holley, E. A., Hartlieb, P., Kaunda, R., & Nelson, P. P. (2018). Methods for characterizing cracks induced in rock. *Rock Mechanics and Rock Engineering*, *51*(7), 2075–2093. https://doi.org/10.1007/s00603-018-1445-x

Palkovic, S. D., Kupwade-Patil, K., Yip, S., & Büyüköztürk, O. (2018). Random field finite element models with cohesive–frictional interactions of a hardened cement paste microstructure. *Journal of the Mechanics and Physics of Solids*, *119*, 349–368. https://doi.org/10.1016/j.jmps.2018.07.007

Salimzadeh, S., Paluszny, A., Nick, H. M., & Zimmerman, R. W. (2018). A three-dimensional coupled thermo-hydro-mechanical model for deformable fractured geothermal systems. *Geothermics*, *71*, 212–224. https://doi.org/10.1016/j.geothermics.2017.09.012

Sha, S., Rong, G., Chen, Z. G., Li, B. W., & Zhang, Z. Y. (2020). Experimental evaluation of physical and mechanical properties of geothermal reservoir rock after different cooling treatments. *Rock Mechanics and Rock Engineering*, *53*(11), 4967–4991. https://doi.org/10.1007/s00603-020-02200-5

Shao, S. S., Ranjith, P. G., Wasantha, P. L. P., & Chen, B. K. (2015). Experimental and numerical studies on the mechanical behaviour of Australian Strathbogie granite at high temperatures: An application to geothermal energy. *Geothermics*, *54*, 96–108. https://doi.org/10.1016/j.geothermics.2014.11.005

Shao, Z. L., Tang, X. H., & Wang, X. G. (2021). The influence of liquid nitrogen cooling on fracture toughness of granite rocks at elevated temperatures: An experimental study. *Engineering Fracture Mechanics*, *246*, 107628. https://doi.org/10.1016/j.engfracmech.2021.107628

Shao, Z. L., Wang, Y., & Tang, X. H. (2020). The influences of heating and uniaxial loading on granite subjected to liquid nitrogen cooling. *Engineering Geology*, *271*, 105614. https://doi.org/10.1016/j.engfracmech.2021.107628

Siegesmund, S., Mosch, S., Scheffzük, C. H., & Nikolayev, D. I. (2008). The bowing potential of granitic rocks: Rock fabrics, thermal properties and residual strain. *Environmental Geology*, *55*(7), 1437–1448. https://doi.org/10.1007/s00254-007-1094-y

Sneddon, I. N. (1965). The relation between load and penetration in the axisymmetric Boussinesq problem for a punch of arbitrary profile. *International Journal of Engineering Science*, *3*(3), 47–56. https://doi.org/10.1016/0020-7225(65)90019-4

Tang, X. H., Zhang, Y. H., Xu, J. J., Rutqvist, J., Hu, M. S., Wang, Z. Z., & Liu, Q. S. (2022). Determining Young's modulus of granite using accurate grain-based modelling with microscale rock mechanical experiments. *International Journal of Rock Mechanics and Mining Sciences*, *157*, 105167. https://doi.org/10.1016/j.ijrmms.2022.105167

Ündül, Ö. (2016). Assessment of mineralogical and petrographic factors affecting petro-physical properties, strength and cracking processes of volcanic rocks. *Engineering Geology*, *210*, 10–22. https://doi.org/10.1016/j.enggeo.2016.06.001

Undul, O., Amann, F., Aysal, N., & Ploetze, M. L. (2015). Micro-textural effects on crack initiation and crack propagation of andesitic rocks. *Engineering Geology*, *193*, 267–275. https://doi.org/10.1016/j.enggeo.2015.04.024

Vandermoledn, I. (1981). The shift of the α–β transition temperature of quartz associated with the thermal expansion of granite at high pressure. *Tectonophysics*, *73*(4), 323–342. https://doi.org/10.1016/0040-1951(81)90221-3

Vázquez, P., Shushakova, V., & Gómez-Heras, M. (2015). Influence of mineralogy on granite decay induced by temperature increase: Experimental observations and stress simulation. *Engineering Geology*, *189*, 58–67. https://doi.org/10.1016/j.enggeo.2015.01.026

Wang, D. B., Bian, X. B., Qin, H., Sun, D. L., & Yu, B. (2021). Experimental investigation of mechanical properties and failure behavior of fluid-saturated hot dry rocks. *Natural Resources Research*, *30*(1), 289–305. https://doi.org/10.1007/s11053-020-09760-x

Wang, F., & Konietzky, H. (2019). Thermo-mechanical properties of granite at elevated temperatures and numerical simulation of thermal cracking. *Rock Mechanics and Rock Engineering*, *52*(10), 3737–3755. https://doi.org/10.1007/s00603-019-01837-1

Wang, F., & Konietzky, H. (2022). Thermal cracking in granite during a heating–cooling cycle up to 1000°C: Laboratory testing and real-time simulation. *Rock Mechanics and Rock Engineering*, *55*(3), 1411–1428. https://doi.org/10.1007/s00603-021-02740-4

Wang, F., Konietzky, H., Frühwirt, T., & Dai, Y. J. (2020). Laboratory testing and numerical simulation of properties and thermal-induced cracking of Eibenstock granite at elevated temperatures. *Acta Geotechnica*, *15*(8), 2259–2275. https://doi.org/10.1007/s00603-021-02740-4

Wong, L. N. Y., & Maruvanchery, V. (2016). Different lithological varieties of Bukit Timah granite in Singapore: A preliminary comparison study on engineering properties. *Rock Mechanics and Rock Engineering*, *49*(7), 2923–2935. https://doi.org/10.1007/s00603-015-0825-8

Wong, L. N. Y., Zhang, Y. H., & Wu, Z. J. (2020). Rock strengthening or weakening upon heating in the mild temperature range? *Engineering Geology*, *272*, 105619. https://doi.org/10.1016/j.enggeo.2020.105619

Wu, F. B., Zhang, D. K., Ma, L. F., Zhao, G. H., Liu, P. T., Zhang, Z. J., et al. (2021). Thermo-hydro-mechanical (THM) evolution law and development of permeability and pore structure of enhanced geothermal systems at ultra-high temperatures. *Geothermics*, *97*, 102253. https://doi.org/10.1016/j.geothermics.2021.102253

Wu, Z. J., Li, M. Y., & Weng, L. (2020). Thermal-stress–aperture coupled model for analyzing the thermal failure of fractured rock mass. *International Journal of Geomechanics*, *20*(10), 4020176. https://doi.org/10.1061/(ASCE)GM.1943-5622.0001809

Xu, J. J., Tang, X. H., Wang, Z. Z., Feng, Y. F., & Bian, K. (2020). Investigating the softening of weak interlayers during landslides using nanoindentation experiments and simulations. *Engineering Geology*, *277*, 105801. https://doi.org/10.1016/j.enggeo.2020.105801

Xu, T., Zhou, G. L., Heap, M. J., Zhu, W. C., Chen, C. F., & Baud, P. (2017). The influence of temperature on time-dependent deformation and failure in granite: A mesoscale modeling approach. *Rock Mechanics and Rock Engineering*, *50*(9), 2345–2364. https://doi.org/10.1007/s00603-017-1228-9

Xu, X. L., & Karakus, M. (2018). A coupled thermo-mechanical damage model for granite. *International Journal of Rock Mechanics and Mining Sciences*, *103*, 195–204. https://doi.org/10.1016/j.ijrmms.2018.01.030

Yang, S. Q., Tian, W. L., Elsworth, D., Wang, J. G., & Fan, L. F. (2020). An experimental study of effect of high temperature on the permeability evolution and failure response of granite under triaxial compression. *Rock Mechanics and Rock Engineering*, *53*(10), 4403–4427. https://doi.org/10.1007/s00603-019-01982-7

Yu, Q. L., Ranjith, P. G., Liu, H. Y., Yang, T. H., Tang, S. B., Tang, C. A., & Yang, S. Q. (2015). A mesostructure-based damage model for thermal cracking analysis and application in granite at elevated temperatures. *Rock Mechanics and Rock Engineering*, *48*(6), 2263–2282. https://doi.org/10.1007/s00603-014-0679-5

Zhang, W. Q., Sun, Q., Hao, S. Q., Geng, J., & Lv, C. (2016). Experimental study on the variation of physical and mechanical properties of rock after high temperature treatment. *Applied Thermal Engineering*, *98*, 1297–1304. https://doi.org/10.1016/j.applthermaleng.2016.01.010

Zhao, Y. S., Wan, Z. J., Feng, Z. J., Xu, Z. H., & Liang, W. G. (2017). Evolution of mechanical properties of granite at high temperature and high pressure. *Geomechanics and Geophysics for Geo-Energy and Geo-Resources*, *3*(2), 199–210. https://doi.org/10.1007/s40948-017-0052-8

Zhao, Z. H. (2016). Thermal influence on mechanical properties of granite: A microcracking perspective. *Rock Mechanics and Rock Engineering*, *49*(3), 747–762. https://doi.org/10.1007/s00603-015-0767-1

Zhong, X., Frehner, M., Kunze, K., & Zappone, A. (2014). A novel EBSD-based finite-element wave propagation model for investigating seismic anisotropy: Application to Finero Peridotite, Ivrea-Verbano zone, northern Italy. *Geophysical Research Letters*, *41*, 7105–7114. https://doi.org/10.1002/2014GL060490

Zhu, W. C., Liu, J., Yang, T. H., Sheng, J. C., & Elsworth, D. (2006). Effects of local rock heterogeneities on the hydromechanics of fractured rocks using a digital-image-based technique. *International Journal of Rock Mechanics and Mining Science*, *43*(8), 1182–1199. https://doi.org/10.1016/j.ijrmms.2006.03.009